

# Light Propagation in Inhomogeneous Universes. IV. Strong Lensing and Environmental Effects.

Premana Premadi<sup>1</sup> and Hugo Martel<sup>2,3</sup>

## ABSTRACT

We study the gravitational lensing of high-redshift sources in a  $\Lambda$ CDM universe. We have performed a series of ray-tracing experiments, and selected a subsample of cases of strong lensing (multiple images, arcs, and Einstein rings). For each case, we identified a massive galaxy that is primarily responsible for lensing, and studied how the various density inhomogeneities along the line of sight (other galaxies, background matter) affect the properties of the image. The matter located near the lensing galaxy, and physically associated with it, has a small effect. The background matter increases the magnification by a few percents at most, while nearby galaxies can increase it by up to about 10 percent. The effect on the image separation is even smaller. The only significant effect results from the random alignment of physically unassociated galaxies, which can increase the magnification by factors of several, create additional images, and turn arcs into rings. We conclude that the effect of environment on strong lensing is negligible in general, and might be important only in rare cases. We show that our conclusion does not depend on the radial density profile of the galaxies responsible for lensing.

*Subject headings:* cosmology: theory — dark matter — galaxies: halos — gravitational lensing — large-scale structure of universe

## 1. INTRODUCTION

The gravitational lensing of sources located at cosmological distances is usually referred to as “strong lensing” or “weak lensing,” depending on the magnitude of the effect. “Strong lensing” refers to cases with multiple images, arcs, or rings, while “weak lensing” refers to the magnification and shear of single images. We can divide the observed cases of strong lensing in two groups. The first group contains the “arc second” cases: multiple-image systems with image separations of order arc seconds, or rings with radii of that order (see Kochanek et al. 1998).<sup>1</sup> In such cases, the lens

---

<sup>1</sup>Department of Astronomy and Bosscha Observatory, Bandung Institute of Technology, Bandung, Indonesia

<sup>2</sup>Department of Astronomy, University of Texas, Austin, TX 78712

<sup>3</sup>Département de physique, de génie physique et d’optique, Université Laval, Québec, Canada, G1K 7P4

<sup>1</sup>See <http://cfa-www.harvard.edu/castles>.

is usually a single, massive galaxy located along or near the line of sight to the source. A classic example is Q0957+561, the first gravitational lens discovered (Walsh, Carswell, & Weymann 1979). The second group contains the “arc minute” cases, in which the lens is an entire cluster of galaxies. These lenses produce mostly giant arcs, with radii in the range  $15'' - 60''$  (see Table 1 of Williams, Navarro, & Bartelmann 1999). The most famous case is the cluster CL 0024+1654, located at redshift  $z = 0.39$ , which produces three main arcs and one counter-arc, with a radius of  $35''$ . Both strong and weak lensing have been used to constrain the cosmological parameters, the spectrum of primordial density fluctuations, and the nature and structure of the lenses (for recent reviews, see Wambsganss 1998; Soucail 2001; Bartelmann & Schneider 2001; Claeskens & Surdej 2002).

In this paper, the fourth of a series on light propagation in inhomogeneous universes, we focus on the arc-second cases of strong lensing that result when a massive galaxy is located along the line of sight to a distant source. If the galaxy were the only density inhomogeneity along the line of sight, a description of its lensing properties would be quite trivial. There is a large body of literature describing the lensing properties of individual galaxies (or more generally “halos”) with particular density profiles, including spherically symmetric profiles (e.g. Hinshaw & Krauss 1987; Schneider, Ehlers, & Falco 1992 [hereafter SEF], §8.1.5; Wright & Brainerd 2000; Rusin & Ma 2001; Martel & Shapiro 2003) and flattened ones (e.g. Schramm 1990; Schneider & Weiss 1991; Keeton & Kochanek 1995). However, treating lensing galaxies in isolation is only a convenient approximation. The presence of other density inhomogeneities along the same line of sight can modify the properties of the image. If a lensing galaxy is located in a dense cluster, the presence of nearby cluster members can modify the magnification or the image separation. Also, the whole cluster might be embedded inside a common dark matter halo (hereafter referred to as the *background component*), whose presence might also have some effect on the lens properties. Strong lensing usually requires a massive elliptical or S0 galaxy, and such galaxies tend to lie in dense environments, as indicated by the morphology-density relation (Dressler 1980). However, it has been suggested that the luminosity distribution of galaxies depends on environment (Bromley et al. 1998; Christlein 2000; Zabludoff & Mulchaey 2000), leading to a ratio of dwarf to giant galaxies that is higher in denser environments. Keeton, Christlein, & Zabludoff (2000) argue that this effect nearly cancels the effect of the morphology-density relation, and predict that only  $\sim 25\%$  of lensing galaxies are located in dense environments. While environmental effects are irrelevant for the remaining  $75\%$  of lenses that do not reside in dense environments, they can certainly be important for the  $25\%$  of lenses located in such environments, and might be necessary to explain the few cases with large angular separations ( $s > 6''$ ) that have been observed (see, e.g., Inada et al. 2003).

Turner, Ostriker, & Gott (1984, hereafter TOG) have considered a simple model in which lensing galaxies, modeled as singular isothermal spheres, are embedded into uniform sheets of background matter. They showed that the effect of the background matter can be important, but also indicated that this effect can be weakened by the presence of low-density regions along the same line of sight. Treating the background matter as a uniform sheet allows an analytical treatment, leading to orders of magnitude estimates, but it is a rather crude representation of the

actual matter distribution in a CDM universe in which large-scale structure forms by the growth of Gaussian random fluctuations. In such universe, the rms density fluctuation  $\sigma_{\text{rms}}$  at a particular scale  $\lambda$  is given by

$$\sigma_{\text{rms}}^2(\lambda) = \frac{1}{2\pi^2} \int_0^\infty P(k)W^2(k\lambda)k^2 dk, \quad (1)$$

where  $P(k)$  is the power spectrum, and  $W$  is the top-hat filter function, given by

$$W(x) = \frac{3}{x^3}(\sin x - x \cos x). \quad (2)$$

In a CDM universe, small scales collapse before large ones, hence there is at any epoch a maximum scale  $\lambda_{\text{max}}$  corresponding to the largest structures one expect to find at that epoch in a typical region of the universe. To estimate  $\lambda_{\text{max}}$ , we make the common assumption that the largest structures found in a representative region of the universe correspond to  $3\sigma$  fluctuations. Then, according to the Press-Schechter approximation, the radius of these structures is given by solving

$$\sigma_{\text{rms}}(\lambda_{\text{max}}) = \frac{\delta_{\text{crit}}}{3} \quad (3)$$

for  $\lambda_{\text{max}}$ , where  $\delta_{\text{crit}} \approx 1.69$ . For a  $\Lambda$ CDM universe, we get  $\lambda_{\text{max}} \approx 23$  Mpc. The typical diameter of the largest objects (voids or clusters) we expect to find in a representative region of the universe is therefore of order  $2\lambda_{\text{max}} \approx 46$  Mpc. Sources that are gravitationally lensed are normally located at cosmological distances that greatly exceeds that scale. Hence, there will be several overdensities and underdensities along the line of sight to any source, and one could expect a near-cancellation of their effects. TOG acknowledge that fact.

Two arguments can be made against this line of reasoning. First, while this near-cancellation is expected for a typical line of sight, it might not occur for an atypical one (this is the argument made by TOG). Second, even though there might be several overdensities and underdensities along the line of sight, their relative contributions to lensing will differ. It is well known that the matter that contributes most to lensing tends to be located about half-way between the source and the observer. To be more quantitative, consider a lens L with projected surface density  $\sigma$ , located along the line of sight to a distant source S. We define the convergence  $\kappa$  of the lens as

$$\kappa = \frac{\sigma}{\sigma_{\text{crit}}}, \quad (4)$$

where  $\sigma_{\text{crit}}$  is the critical surface density, defined by

$$\sigma_{\text{crit}} = \frac{c^2 D_S}{4\pi G D_L D_{LS}}, \quad (5)$$

and  $D_S$ ,  $D_L$ , and  $D_{LS}$  are the angular diameter distance between observer and source, observer and lens, and source and lens, respectively (SEF, p. 158). The value of  $\kappa$  provides an estimate of

the strength of gravitational lensing. We can define a *lensing weight*  $w(z)$  using

$$w(z) = \frac{1}{\sigma_{\text{crit}}} = \frac{4\pi G D_L D_{LS}}{c^2 D_S}. \quad (6)$$

The lensing weight gives a measure of the relative contributions to lensing of matter located at various redshifts  $z$ , all other things being equal. This function is zero at the location of the observer and the source, and peaks at intermediate distances (see Fig. 2 below). The largest contribution to lensing will usually come from matter located in the redshift interval where  $w(z)$  is large. The extent of this region is smaller than the whole distance between source and observer. If it is only a few times  $\lambda_{\text{max}}$ , it will contain only a few overdensities and underdensities, and the cancellation of their effect will not be perfect in general. Notice that this effect is partially compensated by the fact that at redshifts  $z > 0$  where  $w(z)$  peaks, the value of  $\lambda_{\text{max}}$  is smaller than at the present in a CDM universe.

There is a clear need for a more realistic approach to this problem than the uniform-sheet approximation of TOG. A recent attempt to quantify the importance of environmental effects on strong lensing by massive galaxies was presented by Holder & Schechter (2003). These authors used simulated large-scale structure and galaxy distributions (as we do here), identified the most massive galaxies as being the ones capable of producing strong lensing, and calculated, at the location of these galaxies, the gravitational shear caused by nearby large-scale structures and galaxies. They concluded that the typical shear is of order 10 – 15%.

Our goal in this paper is similar. We want to determine the typical magnitude of environmental effects, and demonstrate that very strong effects are rare. However, we consider an approach to this problem that drastically differs from the one used in previous studies. We use a multiple lens-plane algorithm to simulate the actual gravitational lensing of a large number of distant sources. We performed 100 simulations, each simulation producing the images of 841 sources, for a total of 84,100 images. We extract from these simulations a subsample of images that constitute examples of strong lensing, and we reanalyze this subsample on a case-by-case basis. While the original sample of 84,100 images is unbiased and statistically significant, the subsample of 16 cases is strongly biased, since it includes only cases of strong lensing. Such biased sample is ideal for determining an upper limit to the effects of environment on strong lensing.

This work differs from previous studies in our approach to analyzing the effect of the density fluctuations along the line of sight. In particular, instead of focusing on their cumulative effect, we divide these fluctuations in different density components, and determine their relative contributions independently. The most prominent components are clusters of galaxies. We divide these clusters into two components: the galaxies themselves and the diffuse CDM halo in which the galaxies are embedded, and we study the effects of these two components, both individually and in combination. We also consider the effect resulting from the random alignment of galaxies that are physically unassociated.

The remainder of this paper is organized as follow: In §2, we briefly describe our numerical

algorithm. In §3, we describe our original set of simulations, and the 16 cases of strong lensing that we have selected for further analysis. In §4, we identify, for each case, the particular galaxy (referred to as *The Lens*) that is primarily responsible for producing strong lensing. In §5, we investigate the effects of the various density components along the line of sight. In §6, we experiment with variations of the basic model, by considering different density profiles for galaxies. Conclusions are presented in §7.

## 2. THE ALGORITHM

We have developed a *multiple lens-plane algorithm* to study light propagation in inhomogeneous universes (Premadi, Martel, & Matzner 1998, hereafter Paper I; Martel, Premadi, & Matzner 2000; Premadi et al. 2001a, b). Here, we give a brief description of the algorithm. For more details, we refer the reader to Paper I.

In this algorithm, the space between the observer and the source is divided into a series of cubic boxes of comoving size 128 Mpc, and the matter content of each box is projected onto a plane normal to the line of sight. The trajectories of light rays are then computed by adding successively the deflections caused by each plane, using geometrical optics. This method is described in SEF, chapter 9.

To use this algorithm, we need to provide a description of the matter distribution along the line of sight. Matter is divided into two components: background matter and galaxies. We use a P<sup>3</sup>M algorithm to simulate the distribution of background matter. The simulations used 64<sup>3</sup> equal-mass particles and a 128<sup>3</sup> PM grid, inside a comoving volume of size 128 Mpc. We then use a Monte Carlo method for locating galaxies into the computational volume according to the underlying distribution of background matter (Martel, Premadi, & Matzner 1998; Paper I). The distribution of galaxies satisfy several observational constraints, including the two-point correlation function. The luminosities and morphological types of galaxies are chosen according to the Schechter luminosity function (Schechter 1976) and the morphology-density relation (Dressler 1980), respectively. We treat galaxies as nonsingular isothermal spheres, using the models of Jaroszyński (1992). The projected surface density profile of galaxies is given by

$$\sigma(r) = \begin{cases} \frac{v^2}{4G(r^2 + r_c^2)^{1/2}}, & r \leq r_{\max}; \\ 0, & r > r_{\max}; \end{cases} \quad (7)$$

where  $r$  is the projected distance from the center,  $v$  is the rotation velocity,  $r_c$  is the core radius, and  $r_{\max}$  is a truncation radius introduced to prevent the mass from diverging. The parameters  $v$ ,  $r_c$ , and  $r_{\max}$  are functions of the galaxy luminosity and morphological type, given by

$$r_c = r_{c,0}(L/L_*) , \quad (8)$$

$$r_{\max} = r_{\max,0}(L/L_*)^{1/2} , \quad (9)$$

$$v = v_0(L/L_*)^\gamma, \quad (10)$$

where  $L_*$  is the characteristic luminosity of the Schechter luminosity function, and the parameters  $r_{c,0}$ ,  $r_{\max,0}$ ,  $v_0$ , and  $\gamma$  are given in Table 1. The values of  $v_0$  and  $\gamma$  are based on the Faber-Jackson relation for early-type galaxies (Faber & Jackson 1976; de Vaucouleur & Olson 1982) and the Tully-Fisher relation for spiral galaxies (Tully & Fisher 1988; Fukugita et al. 1991). Equations (8) and (9) are based on the studies of Kormendy (1987) and Holmberg (1973), respectively. We refer the reader to Jaroszyński (1992) for details.

### 3. INITIAL SIMULATIONS

We consider a flat, untilted, COBE-normalized  $\Lambda$ CDM model with density parameter  $\Omega_0 = 0.3$ , cosmological constant  $\lambda_0 = 0.7$ , Hubble constant  $H_0 = 65 \text{ km s}^{-1} \text{ Mpc}^{-1}$ , baryon density parameter  $\Omega_b = 0.019h^{-2}$ , and CMB temperature  $T_{\text{CMB}} = 2.73$ . The CDM power spectrum of density fluctuations is described by the transfer function of Bardeen et al. (1986) with the normalization of Bunn & White (1997). These simulations are part of the Texas P<sup>3</sup>M database (Martel & Matzner 2000; El-Ad et al. 2002), and are publicly available. We performed a series of 100 ray-tracing experiments, each experiment consisting of propagating a square beam of angular size  $21.9'' \times 21.9''$  containing  $341^2$  rays, from the observer to the source plane, located at redshift  $z_S = 3$ . These experiments altogether produced images of 84,100 sources of angular diameter  $1''$  located at redshift  $z_S = 3$ . We selected for further analysis a subsample of 16 images that represent cases of strong lensing. These images are shown in Figure 1. Each case is labeled by a letter, from A to P. Our sample includes double images (cases E, F, G, I, J, K), triple images (cases A and C), an Einstein ring (case H), two-hole rings (cases D and N), and more complex images resulting from multiple deflections (Cases B, L, M, O, and P).

### 4. IDENTIFYING THE LENS

We assume that in each case selected, strong lensing results from the presence of a massive galaxy along the line of sight. We shall refer to this galaxy as *The Lens* (with capital initials). To identify it, we pick the ray closest to the center of the source (the “central ray”), and follow the trajectory of that ray from the source to the observer, to find which galaxies are directly hit by this ray. If only one galaxy is hit, this galaxy is identified as The Lens. If several galaxies are hit, we compute for each galaxy the convergence  $\kappa(\mathbf{x})$  at the position  $\mathbf{x}$  on the lens plane where the ray hits the galaxy, using equation (4). The convergence provides a direct estimate of the strength of gravitational lensing. The galaxy that produces the largest value of the convergence at the location of the central ray is identified as The Lens.

Figure 2 shows the masses and redshifts of the galaxies being hit, for all 16 cases. For each case,

the red bar shows The Lens, while the blue bars show the other galaxies. For cases E and L, The Lens is the only galaxy being hit. The solid curves show the lensing weight  $w(z) \equiv 1/\sigma_{\text{crit}}$ , which measures the relative contribution to lensing of matter located at various redshifts. The lensing weight peaks in the region  $z = [0.8, 1.0]$ , about half way between the source and the observer. Not surprisingly, The Lens tends to be found in this region, the only exception being for case M, where The Lens is much closer to the source, at redshift  $z_L = 1.80$ . The Lens is not always the most massive galaxy being hit. In particular, for cases G, M, and N, a galaxy much more massive than The Lens was hit, but it was located near the source and therefore had a small contribution. For case P, two galaxies located at the same redshift are hit, and the least massive is identified as The Lens, because that galaxy is hit near its center, where the projected surface density  $\sigma$  is the largest, while the other galaxy is hit near its outskirts, where the projected surface density is small.

## 5. EFFECT OF THE VARIOUS COMPONENTS

### 5.1. Images, Magnification, and Image Separation

For each case, we identify four components that contribute or might contribute to gravitational lensing: (1) The Lens itself, (2) the galaxies located on the same lens plane, (3) the background matter located on the same plane, and (4) the galaxies and background matter located on other planes. Consecutive lens planes represent regions separated by a comoving distance of 128 Mpc. This greatly exceeds the characteristic scale of both the galaxy-galaxy and cluster-cluster 2-point correlation functions, as well as the scale  $\lambda_{\text{max}}$  discussed in §1. Hence, matter located on different lens planes is physically unassociated, and this fact is built into the ray-tracing algorithm: consecutive lens planes are generated by different N-body simulations, and are given random shifts (Paper I). This is a standard technique to ensure that the structures in neighboring planes are uncorrelated.

All these components were included in the original simulations described in §3. We redid these simulations for our 16 selected cases, turning on only certain components at a time, to estimate their effect. These simulations included (a) Lens only, (b) Lens + galaxies on same plane, (c) Lens + background matter on same plane, and (d) Lens + galaxies and background matter on same plane. The results are shown in Figure 3, along with the results of our original “all planes” simulations. The striking result is that the effect of the background matter and other galaxies on the same plane is very small. Except for cases B, K, and P, it is hardly noticeable. Figure 4 shows the magnification  $\mu$  for all cases. Differences between squares and triangles show the effect of the background matter. Differences between open and filled symbols show the effect of the galaxies. Differences between asterisks and filled squares show the effect of the other lens planes. Figure 5 shows the image separation  $s$  for the 10 cases A, C–G, I–K, and N that produce multiple images. The separations are measured between the center of each image. For cases with more than 2 images (such as case A), the separation is measured between the two outermost images. For cases D and

N, no asterisks are plotted because these cases do not produce multiple images when all planes are included.

From Figures 4 and 5, we can estimate the effect of the various components. The effect of the background matter on the magnification is of order 1% at most, while the effect of the galaxies is of order 10% at most. The exceptions are cases L and M, for which the effect of galaxies is less than 1%, while the effect of the background matter is  $\sim 4\%$  for case L and  $\sim 6\%$  for case M. The presence of galaxies near The Lens tends to increase the magnification. However, for cases B, K, and N we find the opposite effect: the magnification is reduced. The effect of these components on the image separation tends to be very small. It exceeds 2% for three cases only, D, F, and K. In all three cases, it is the galaxies that are responsible for the effect. Notice that in cases D and F, the effect is a reduction of the image separation. The largest effect seen in Figures 4 and 5 result from the presence of the other lens planes. In 6 cases out of 16 (A, C, D, M, N, and O), the magnification more than doubles when the other lenses planes are included. For cases A and C, a third image appears, resulting in a significant increase of the image separation.

## 5.2. The Non-effect of the Background Matter

To understand the effect of the background matter, we computed the volume density of background matter along the line of sight, in the vicinity of The Lens. The resulting density profiles are shown in Figure 6 (solid curves), where the density is plotted along an interval of comoving length 128 Mpc centered on The Lens, that is, going from 64 Mpc in front of The Lens to 64 Mpc behind it. Except for cases E and M, The Lens was always located in a dense region. This was expected, since our algorithm locates galaxies predominantly in clusters, where the density of dark matter is large. Only for cases E and M The Lens is a field galaxy.

When The Lens is located in a cluster, the large overdensity of background matter increases the effect of lensing. However, this effect is greatly compensated by the presence of low-density regions along the line of sight. The dashed lines show the line-of-sight-averaged background density within a distance of  $\pm 64$  Mpc (comoving) from The Lens. The values are not particularly large, the maximum being  $2.89\bar{\rho}$  for cases B, C, and D (where  $\bar{\rho}$  is the universal mean density), while for cases A and K, the line-averaged value is actually *less* than the mean value! This illustrates the point that was made in §1, and that was also made by TOG: along any line of sight, there will be several overdense and underdense regions, and their effects will cancel out at least partly. As Figure 6 shows, the clusters where The Lenses are located tend to be surrounded by underdense regions (solid curve dipping below the dotted line). The only cases where the locally-averaged background density was more than 100% larger than the universal background density ( $\rho/\bar{\rho} > 2$ ) are cases B, C, D, and L. Case L turns out to be one of the few cases for which the effect of the background matter exceeds the effect of the galaxies, as Figure 4 shows.

### 5.3. The Non-effect of the Galaxies

Since The Lens tends to be located in a dense cluster, we expect to find many galaxies nearby. However, only in two cases, D and P, a second galaxy located in the same plane as The Lens was directly hit (see Fig. 2). The geometric cross-section of galaxies,  $\sigma_{\text{geom}} = \pi r_{\text{max}}^2$ , is sufficiently small that galaxies located on the same plane do not overlap much when seen in projection. This point was already made in Paper II (see Fig. 10 in that paper). Hence, if the galaxies physically associated with The Lens (that is, belonging to the same cluster) have any effect at all, it will usually result from their combined tidal field. For this effect to be important, two conditions must be satisfied: (i) The combined mass of these galaxies must be important, and (ii) their distribution around The Lens must be asymmetric.

To identify the cluster in which The Lens belong, we simply find all galaxies located inside a sphere of comoving radius  $R = 5 \text{ Mpc}$  centered around The Lens. This value of 5 Mpc corresponds roughly to the half-width of the density peaks seen in Figure 6, and can therefore be used as a fiducial cluster radius. The galaxies found inside that sphere are considered to be members of the same cluster as The Lens. Notice that even though The Lens is located in the center of the sphere used to identify cluster members, it is not necessarily located in the center of the cluster itself. In Table 2, we give, for each case, the number of galaxies  $N$  in the cluster, the mass  $M_{\text{Lens}}$  of The Lens, the total mass  $M_{\text{total}}$  of the galaxies in the cluster, the ratio  $M_{\text{Lens}}/M_{\text{total}}$ , and the rank of The Lens, where rank  $n$  means that The Lens is the  $n^{\text{th}}$  most massive galaxy in the cluster. Except of cases B, C, D, L, and M, the mass in The Lens is a small fraction of the total cluster mass, less than 10%. Of course, The Lens is directly hit by the beam, while other galaxies contribute only by their tidal fields. Consequently, even though The Lens does not dominate the mass of the cluster, it is the most dominant lensing component.

The Lens is the most massive galaxy in the cluster for 5 cases, and among the five most massive galaxies for 13 cases out of 16, the exceptions being cases N, O, and P. Figure 4 shows that these three cases are among the ones for which the effect of galaxies is the largest, with an increase in magnification larger than 10% for case P. Notice the large distortion of the image seen in Figure 3 for that particular case, when galaxies are added.

The non-effect of galaxies near The Lens results primarily from the cancellation of their tidal fields. Since The Lens is usually one of the most massive galaxy in the cluster, it tends to be located near the cluster center, a consequence of mass segregation.<sup>2</sup> In that case, the other galaxies in the cluster surround The Lens, leading to a substantial cancellation of their tidal fields.

---

<sup>2</sup>In our algorithm, mass segregation is not achieved dynamically, but is a mere consequence of morphological segregation. Galaxies located near the center of clusters are predominantly early-types, and they tend to be more massive than spirals (see larger values of  $v_0$  in Table 1).

## 6. VARYING THE LENS DENSITY PROFILE

Our ray-tracing algorithm treats galaxies as nonsingular isothermal spheres. Each galaxy is described by three parameters, the core radius  $r_c$ , maximum radius  $r_{\max}$ , and rotation velocity  $v$ , which are related to the galaxy luminosity and morphological type according to equations (8)–(10). In this section, we investigate the dependence of our results upon this particular choice, by considering other density profiles.

### 6.1. Singular Isothermal Sphere

The simplest profile to consider is the singular isothermal sphere. To obtain this profile, we simply set  $r_c = 0$  in equation (7). Hence, we are essentially replacing every galaxy in our simulation by a singular isothermal sphere with the same rotation velocity and maximum radius.

### 6.2. NFW Profile and Truncated Isothermal Sphere

We also consider two other density profiles. The first one is the widely-used Navarro-Frenk-White (NFW) profile (Navarro, Frenk, & White 1997), given by

$$\rho(r) = \frac{\rho_{\text{NFW}}}{(r/r_{\text{NFW}})(r/r_{\text{NFW}} + 1)^2}, \quad (11)$$

where  $r_{\text{NFW}}$  and  $\rho_{\text{NFW}}$  are a characteristic radius and density, respectively. The second one is the Truncated Isothermal Sphere (TIS), a model that was derived by Shapiro, Iliev, & Raga (1999) and Iliev & Shapiro (2001). These authors computed the minimum-energy solution of the isothermal Lane-Emden equation, modified to account for accretion by cosmological infall. The actual solution can only be obtained numerically, but is well-approximated by the following expression,

$$\rho(r) = \rho_{\text{TIS}} \left( \frac{A}{a^2 + r^2/r_{\text{TIS}}^2} - \frac{B}{b^2 + r^2/r_{\text{TIS}}^2} \right), \quad (12)$$

where  $r_{\text{TIS}}$  and  $\rho_{\text{TIS}}$  are a characteristic radius and density, respectively, and  $A = 21.38$ ,  $B = 19.81$ ,  $a = 3.01$ ,  $b = 3.82$  (Shapiro et al. 1999). The lensing properties of the NFW profile and TIS are described in great details by Martel & Shapiro (2003, and references therein).

The parameters  $r_{\text{NFW}}$ ,  $\rho_{\text{NFW}}$ ,  $r_{\text{TIS}}$  and  $\rho_{\text{TIS}}$  are not free parameters, but functions of the halo mass, redshift, and the cosmological model (Navarro et al. 1997; Shapiro et al. 1999; Eke, Navarro, & Steinmetz 2001; Iliev & Shapiro 2001). However, these models are based on theoretical assumptions that are inconsistent with the approach we used to generate the distributions of galaxies (see Paper I). Consequently, we will treat the characteristic radii and densities as free parameters, thus treating the NFW profile and the TIS as mere fitting formulae. The problem is then the following:

considering a galaxy represented as a nonsingular isothermal sphere described by equation (7)–(10), we need to derive expressions relating the characteristic radius and density to  $r_c$ ,  $r_{\max}$ , and  $v$ , such that the same galaxy can be represented as either a NFW profile or a TIS. Since each profile has two parameters, we need to impose two constraints. First, the characteristic radii are related to the tidal radius  $r_{200}$  by  $r_{\text{NFW}} = r_{200}/C$  and  $r_{\text{TIS}} = r_{200}/\zeta_{200}$ , where  $C$  and  $\zeta_{200}$  are functions of the halo mass, redshift, and the cosmological model (for  $\zeta_{200}$ , the dependence is weak). We assume that the tidal radius  $r_{200}$  is equal to the maximum radius  $r_{\max}$ .<sup>3</sup> For the NFW profile, we use a fixed value  $C = 9$ , which is the value predicted by the NFW model for a halo of mass  $M \sim 2 \times 10^{12} M_\odot$  at redshift  $z \sim 0.6$  in a  $\Lambda$ CDM universe. This value is therefore reasonable for the galaxies we have identified as “The Lens.” For the TIS profile, we use the canonical value  $\zeta_{200} = 24.2$ , which is correct for all halos in an Einstein-de Sitter universe. As Iliev & Shapiro (2001) showed, the dependence of  $\zeta_{200}$  on the cosmological parameters is weak, so using this value for a  $\Lambda$ CDM universe is not a bad approximation.

This fixes the values of the characteristic radii  $r_{\text{NFW}}$  and  $r_{\text{TIS}}$ . Our second assumption is that the rotation velocity  $v_{\text{rot}}$  at radius  $r = r_{\max}$  is the same for all profiles. This ensures that the mass of each galaxy remains fixed, no matter what density profile is considered. The rotation velocities are given by

$$v_{\text{rot}}^2(r) = \frac{4\pi G \rho_{\text{NFW}} r_{\text{NFW}}^3}{r} \left[ \ln(1 + r/r_{\text{NFW}}) - \frac{r/r_{\text{NFW}}}{1 + r/r_{\text{NFW}}} \right], \quad (\text{NFW}); \quad (13)$$

$$v_{\text{rot}}^2(r) = 4\pi G \rho_{\text{TIS}} r_{\text{TIS}}^2 \left[ A - B - \frac{aAr_{\text{TIS}}}{r} \arctan \frac{r}{ar_{\text{TIS}}} + \frac{bBr_{\text{TIS}}}{r} \arctan \frac{r}{br_{\text{TIS}}} \right], \quad (\text{TIS}); (14)$$

(Chiba & Takahashi 2002; Martel & Shapiro 2003). We set  $r = r_{\max}$ , equate these expressions to  $v^2$ , and solve for the characteristic densities. We get

$$\rho_{\text{NFW}} = \frac{Cv^2}{4\pi Gr_{\text{NFW}}^2} \left[ \ln(1 + C) - \frac{C}{1 + C} \right]^{-1}, \quad (15)$$

$$\rho_{\text{TIS}} = \frac{v^2}{4\pi Gr_{\text{TIS}}^2} \left[ A - B - \frac{aA}{\zeta_{200}} \arctan \frac{\zeta_{200}}{a} + \frac{bB}{\zeta_{200}} \arctan \frac{\zeta_{200}}{b} \right]^{-1}. \quad (16)$$

Once the parameters  $r_{\text{NFW}}$ ,  $\rho_{\text{NFW}}$ ,  $r_{\text{TIS}}$ , and  $\rho_{\text{TIS}}$  are determined, it is straightforward to implement these density profiles into the ray-tracing algorithm, using the expressions given by Chiba & Takahashi (2002) and Martel & Shapiro (2003) for the deflection angle.

We selected the particular cases B, C, J, and P, and redid all experiments, using the various density profiles. Figure 7 shows the ratio  $\mu/\mu_{\text{Lens}}$  for these experiments. The results are consistent with the ones shown in Figure 4. The effect of the background matter is of order 1% at most, the

---

<sup>3</sup>The TIS actually has a truncation radius  $r_t \approx 1.2r_{200}$ . Setting that truncation radius equal to  $r_{\max}$  would be an alternative.

effect of the galaxies is of order 10% at most, and the effect of the other lens planes can be a factor of several. The only exception is case P with the TIS profile, where the effect of the galaxies (solid symbols) is of order 40%.

## 7. SUMMARY AND CONCLUSION

We have performed a series of ray-tracing experiments using a multiple lens-plane algorithm. We selected 16 cases of strong lensing. By following the trajectory of the beam from the source to the observer, we were able to determine which galaxies along the line of sight were directly hit by the beam. The galaxy that produced the largest value of the convergence  $\kappa$  was identified as The Lens, the galaxy primarily responsible for strong lensing. Our objective was then to study the effects and relative importance of the various components along the line of sight, including (i) The Lens itself, (ii) the galaxies located at the same redshift as The Lens, and possibly associated with it (i.e. in the same cluster), (iii) the background matter located at the same redshift as The Lens, and (iv) the matter located at different redshifts.

With the exception of case M, The Lens was always located in the redshift interval  $0.3 \leq z \leq 1.1$ , where the lensing weight  $w(z) = 1/\sigma_{\text{crit}}$  is large (see Fig. 2). With the exception of cases E and M, The Lens was always in a region where the background density is large (see Fig. 6). This was expected; strong lensing is caused by massive elliptical and S0 galaxies, which tend to be located in dense environments according to the morphology-density relation. In 13 cases out of 16, The Lens was among the 5 most massive galaxies within a comoving distance of 5 Mpc.

The effect of the galaxies and background matter associated with The Lens are rather small. The magnifications and image separations vary by  $\sim 1\%$  when the background matter is added, and  $\sim 10\%$  when the galaxies are added, for all cases. In some cases (B, K, and P), a deformation of the image is clearly visible (Fig. 3). Adding the other lens planes produces effects that range from insignificant to spectacular. Insignificant effects occur when The Lens is the only large mass concentration hit by the beam, while spectacular effects occur when several galaxies are hit by the beam, including galaxies as massive or more massive than The Lens. The presence of additional galaxies along the line of sight can create additional images (cases A, M, and O), turn arcs into rings (cases D and N), and cause large increases in magnification, up to factors of several. The effect of the other lens planes on the image separation is less spectacular, but the accumulated effect is still larger than the effect of the galaxies and background matter associated with The Lens.

Based on these results, we can summarize the effect of the various components along the line of sight, relative to the effect of The Lens itself, as follows:

- Background matter located near The Lens: a few percent (difference between squares and triangles in Figs. 4 and 8).
- Galaxies near The Lens: several percents, up to 10–15% (cases K and P) (differences between

open and filled symbols in Figs. 4 and 8).

- Galaxies and background matter on other planes: factor of several (difference between filled squares and asterisks in Figs. 4 and 8).

We conclude that environmental effects usually play a minor role in strong gravitational lensing. The large magnification associated with strong lensing results primarily from a single, massive galaxy (The Lens), or from the random alignment of several physically unassociated galaxies at different distances. It is important to insist that this conclusion is restricted to strong lensing, and cannot be generalized to weak lensing. We showed that environmental effects can be of order 10%. If, say, a massive galaxy, acting as a lens, increases the brightness of a distant source by 10%, and the nearby galaxies and background matter increase it by an additional 10%, the net effect is increased by a factor of 2. Hence, environmental effects can be very important for weak lensing, but are usually not important for strong lensing. We have experimented with various density profiles of galaxies, and reached the same conclusion. In all these experiments, *we have not found one single case for which the nearby background matter or nearby galaxies make any significant difference.*

One could debate the statistical significance of our results. We have considered a subsample of 16 images. Had we considered a larger subsample, we might have found a case for which environmental effects are important. For instance, we might find a cluster containing two massive galaxies that happen to be aligned with the source, so that the beam hits both galaxies near their center. In this case, one galaxy would be identified as The Lens, and the effect of the other galaxy would be very important. Such cases must be very rare, though. The fact that a subsample of 16 cases has not turned up one single case for which environmental effects are important, in spite of the fact that our sample only included cases of very strong lensing, suggests that any case for which such effects are important must be atypical. In this, we reach the same conclusion as TOG. Note that this results justifies *a posteriori* our approach of using a biased subsample of 16 cases. If we had found, say, 10 or 11 cases for which environmental effects were very strong, the whole approach would have broken down, but no such cases were found.

All calculations were performed at the Texas Advanced Computing Center, University of Texas. This work was supported by NASA ATP Grants NAG5-10825, NAG5-10826, and NAG5-13271. HM thanks the Canada Research Chair program for support.

## REFERENCES

- Bardeen, J. M., Bond, J. R., Kaiser, N., & Szalay, A. S. 1986, *ApJ*, 304, 15
- Bartelmann, M., & Schneider, P. 2001, *Phys. Rep.*, 340, 291
- Bunn, E. F., & White, M. 1997, *ApJ*, 480, 6
- Bromley, B. C., Press, W. H., Lin, H., & Kirshner, R. P. 1998, *ApJ*, 505, 25
- Chiba, T., & Takahashi, R. 2002, *Prog. Theor. Phys. Lett.*, 107, 625
- Christlein, D. 2000, *ApJ*, 545, 145
- Claeskens, J.-F., & Surdej, J. 2002, *A&A Rev.*, 10, 263
- de Vaucouleur, G., & Olson, G. W. 1982, *ApJ*, 256, 346
- Dressler, A. 1980, *ApJ*, 236, 351
- Eke, V. R., Navarro, J. F., & Steinmetz, M. 2001, *ApJ*, 554, 114
- El-Ad, H., Martel, H., Lecar, M., & Piran, T. 2002, *ApJ*, 565, 649
- Faber, S. M., & Jackson, R. 1976, *ApJ*, 204, 668
- Fukugita, M., Okamura, S., Tarusawa, K., Rood, H. J., & Williams, B. A. 1991, *ApJ*, 376, 8
- Hinshaw, G., & Krauss, L. M. 1987, *ApJ*, 320, 468
- Holder, G. P., & Schechter, P. L. 2003, *ApJ*, 589, 688
- Holmberg, E. 1973, in *Galaxies and the Universe*, eds. A. Sandage, M. Sandage, & J. Kristian (Chicago: The University of Chicago Press), p. 123
- Iliev, I. T., & Shapiro, P. R. 2001, *MNRAS*, 325, 468
- Inada, N. et al. 2003, *Nature*, 426, 810
- Jaroszyński, M. 1992, *MNRAS*, 255, 655
- Keeton, C. R., Christlein, D., & Zabludoff, A. I. 2000, *ApJ*, 545, 129
- Keeton, C. R., & Kochanek, C. S. 1998, *ApJ*, 495, 157
- Kochanek, C. S., Falco, E. E., Impey, C., Lahár, J., McLeod, B., & Rix, H.-W. 1998, *CASTLE Survey Gravitational Lens Data Base* (Cambridge: CfA).
- Kormendy, J. 1987, in *Dark Matter in the Universe*, IAU Symposium No 117, eds. J. Kormendy & G. R. Knapp (Dordrecht: Reidel), p. 139

- Martel, H., & Matzner, R. 2000, *ApJ*, 530, 525
- Martel, H., Premadi, P., & Matzner, R. 1998, *ApJ*, 497, 512
- Martel, H., Premadi, P., & Matzner, R. 2000, *ApJ*, 537, 28
- Martel, H., & Shapiro, P. R. 2003, preprint (astro-ph/0305174)
- Navarro, J. F., Frenk, C. S., & White, S. D. M. 1997, *ApJ*, 490, 493
- Premadi, P., Martel, H., & Matzner, R. 1998, *ApJ*, 493, 10 (Paper I).
- Premadi, P., Martel, H., Matzner, R., & Futamase, T. 2001a, *ApJS*, 135, 7
- Premadi, P., Martel, H., Matzner, R., & Futamase, T. 2001b, *Pub.A.S.Aus*, 18, 201
- Rusin, D., & Ma, C.-P. 2001, *ApJ*, 549, L33
- Schechter, P. L. 1976, *ApJ*, 203, 297
- Schneider, P., Ehlers, J., & Falco, E. E. 1992, *Gravitational Lenses* (New York: Springer) (SEF)
- Schneider, P., & Weiss, A. 1991, *A&A*, 247, 269
- Schramm, T. 1990, *A&A*, 231, 19
- Shapiro, P. R., Iliev, I. T., & Raga, A. C. 1999, *MNRAS*, 307, 203
- Soucail, G. 2001, in *Relativistic Astrophysics*, eds. J. C. Wheeler & H. Martel (AIP Conference Proceedings, no 586), p. 233
- Tully, R. B., & Fisher, J. R. 1977, *A&A*, 54, 661
- Turner, E. L., Ostriker, J. P., & Gott, J. R. 1984, *ApJ*, 284, 1 (TOG)
- Walsh, D., Carswell, R. F., & Weymann, R. J. 1979, *Nature*, 279, 381
- Wambsganss, J. 1998, *Living Reviews in Relativity*, 1998-12
- Williams, L. L. R., Navarro, J. F., & Bartelmann, M. 1999, *ApJ*, 527, 535
- Wright, C. O., & Brainerd, T. G. 2000, *ApJ*, 534, 34
- Zabludoff, A. I., & Mulchaey, J. S. 2000, *ApJ*, 539, 136

Table 1. Galaxy Parameters

Type	$r_0$ ( $h^{-1}\text{kpc}$ )	$r_{\text{max}0}$ ( $h^{-1}\text{kpc}$ )	$v_0$ ( $\text{km s}^{-1}$ )	$\gamma$
Elliptical	0.1	30	390	0.250
S0	0.1	30	357	0.250
Spiral	1.0	30	190	0.381

Table 2. Galaxies near The Lens

Case	$N(< 5 \text{ Mpc})$	$M_{\text{Lens}}[10^{12}M_{\odot}]$	$M_{\text{total}}[10^{12}M_{\odot}]$	$M_{\text{Lens}}/M_{\text{total}}$	Rank
A	70	1.15	16.11	0.071	5
B, C, D	44	3.59	21.81	0.164	2
E	82	2.40	27.34	0.088	3
F	101	1.31	24.69	0.053	3
G	101	1.92	29.29	0.066	2
H, I, J	318	4.64	104.76	0.044	1
K	36	3.05	12.96	0.235	1
L	118	1.89	30.04	0.063	1
M	40	2.28	10.98	0.208	2
N	254	1.10	87.10	0.013	22
O	164	0.87	38.87	0.022	14
P	148	0.62	35.17	0.018	18

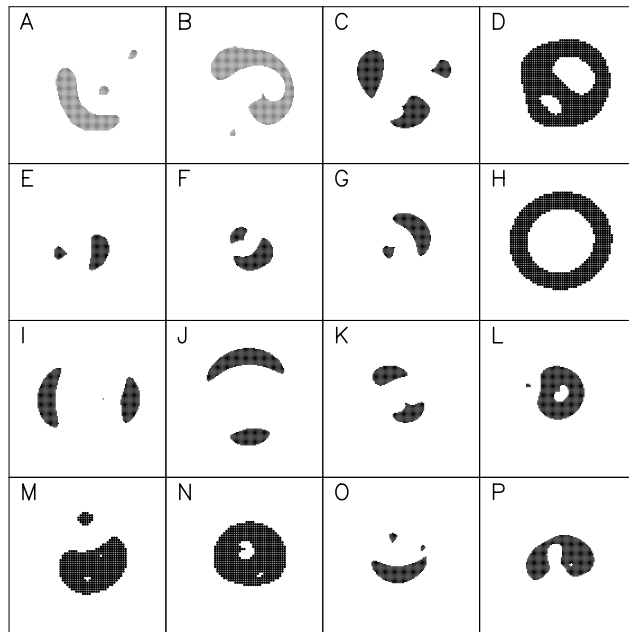


Fig. 1.— All-plane lensing images of the 16 particular cases we have selected for further analysis. These cases include double images (B, E, F, G, I, J, and K), triple images (A, C, and O), Einstein ring (H), rings with secondary image (L and M), double rings (D and N), and peculiar image (P). All panels are  $9'' \times 9''$  in size.

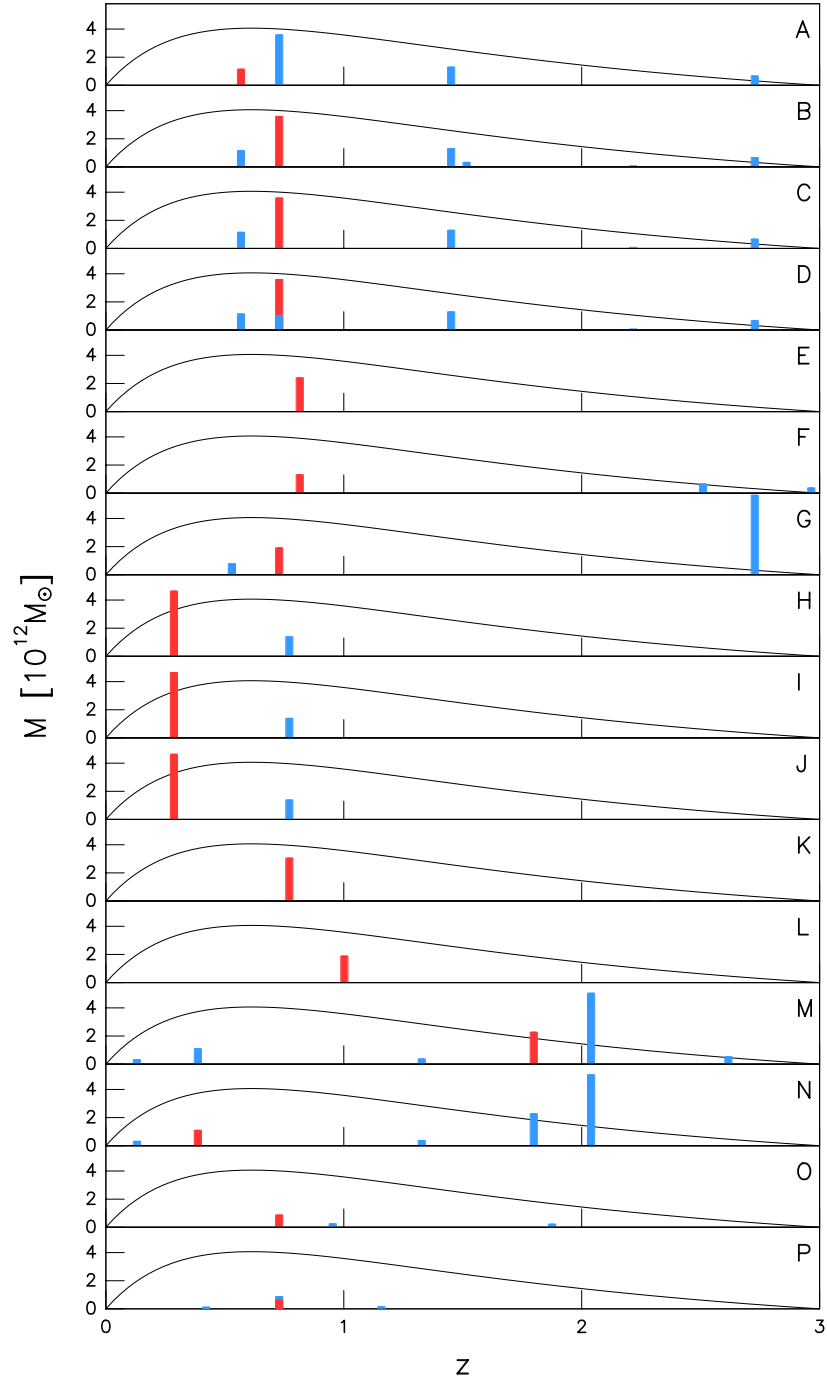


Fig. 2.— Bar diagram showing the mass of the galaxies that are hit by the source’s central ray, versus redshift. The red bar indicates the galaxy that was identified as The Lens. Blue bars indicate the other galaxies. The solid curves show the quantity  $1/\sigma_{\text{crit}}$ , in arbitrary units.

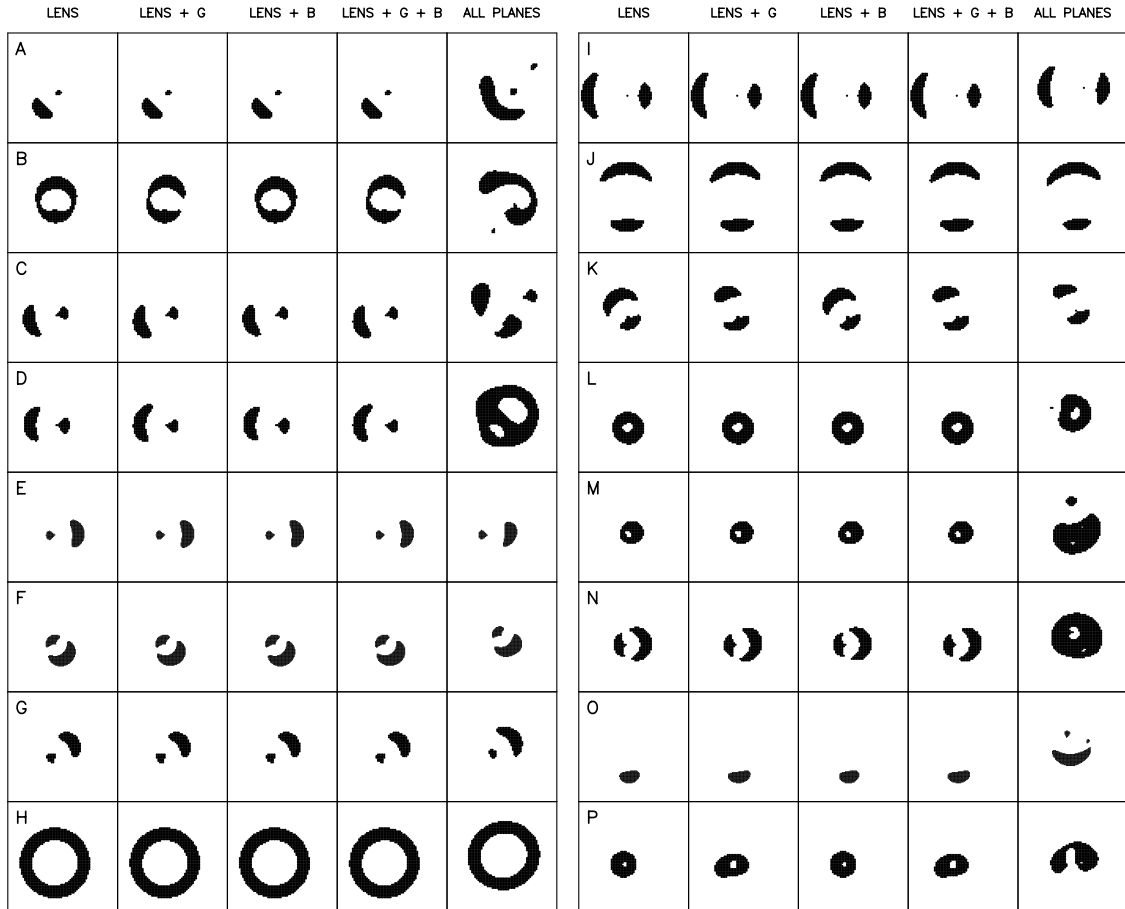


Fig. 3.— Images resulting from lensing by various components. Each row corresponds to a particular case, labeled A through P. First column: Lens only; second column: Lens + galaxies on same plane; third column: Lens + background matter on same plane; fourth column: Lens + galaxies and background matter on same plane; fifth column: all planes included.

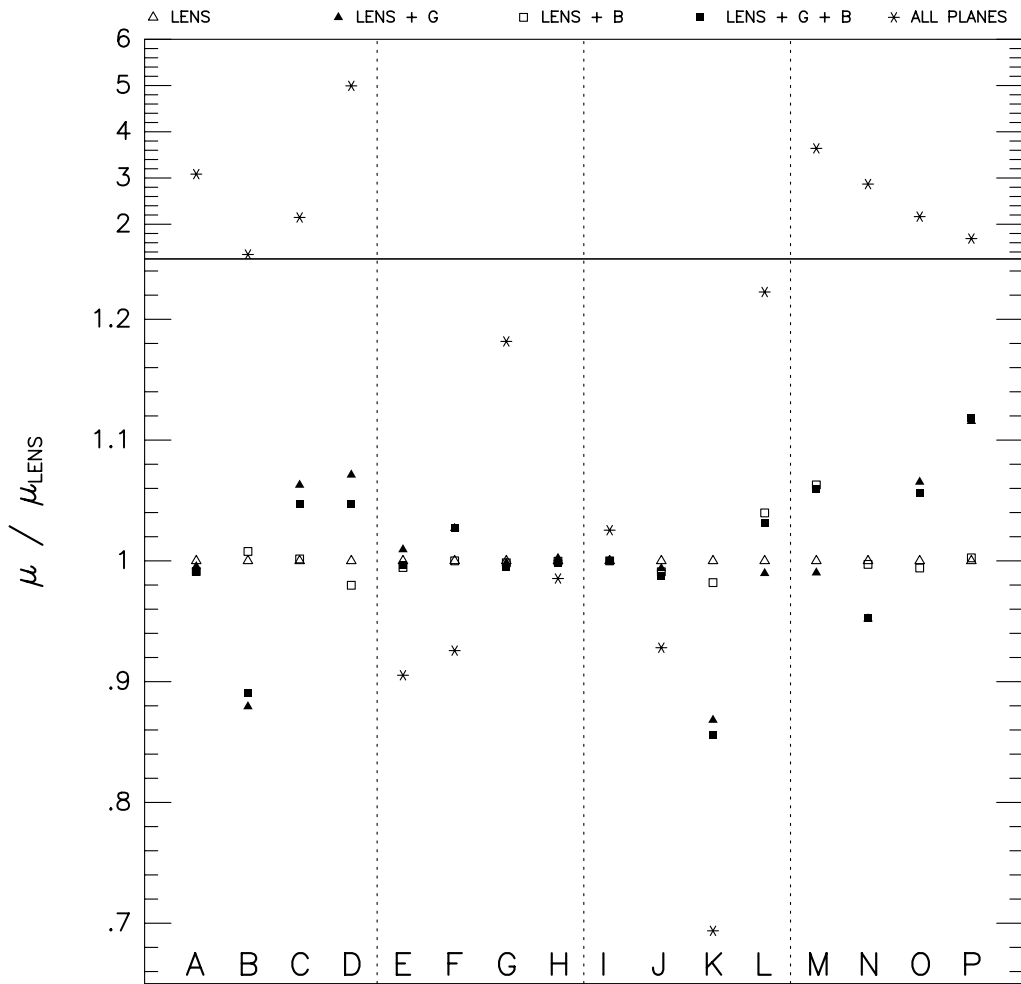


Fig. 4.— Ratio  $\mu/\mu_{\text{LENS}}$ , where  $\mu$  is the magnification and  $\mu_{\text{LENS}}$  is the value of  $\mu$  for the Lens case. The various symbols correspond to various types of experiments, as labeled. The various cases are identified by the letters at the bottom of the figure.

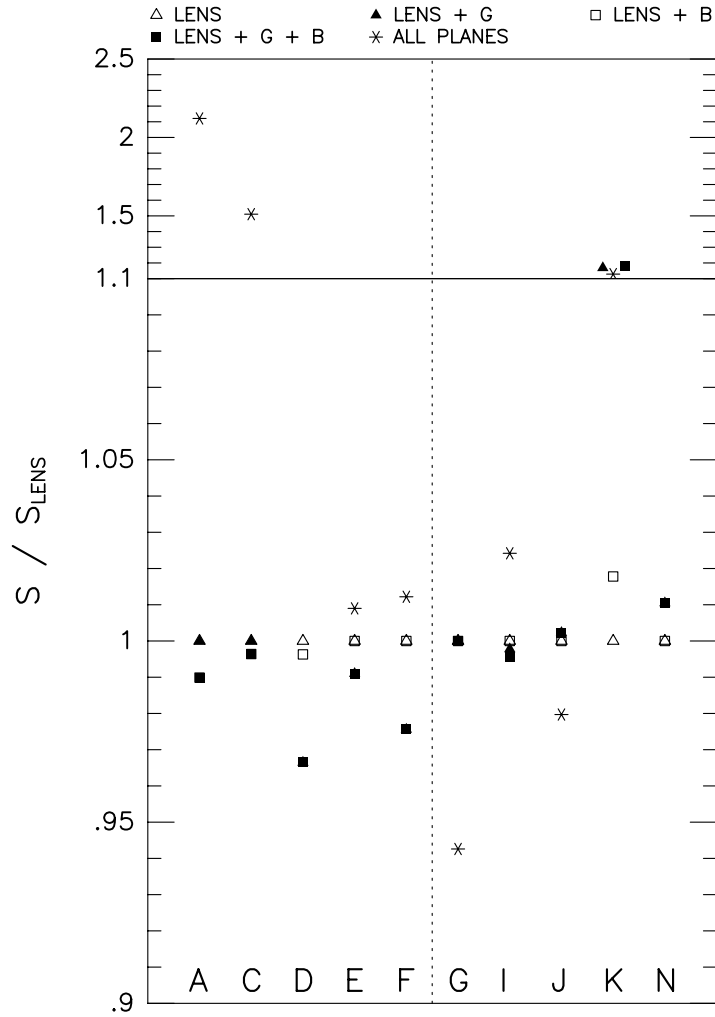


Fig. 5.— Ratio  $s/s_{\text{Lens}}$ , where  $s$  is the image separation and  $s_{\text{Lens}}$  is the value of  $s$  for the Lens case. The various symbols correspond to various types of experiments, as labeled. The various cases are identified by the letters at the bottom of the figure (Cases B, H, L, M, O, and P do not produce multiple images). For case K, we have displaced the filled symbols sideways for clarity.

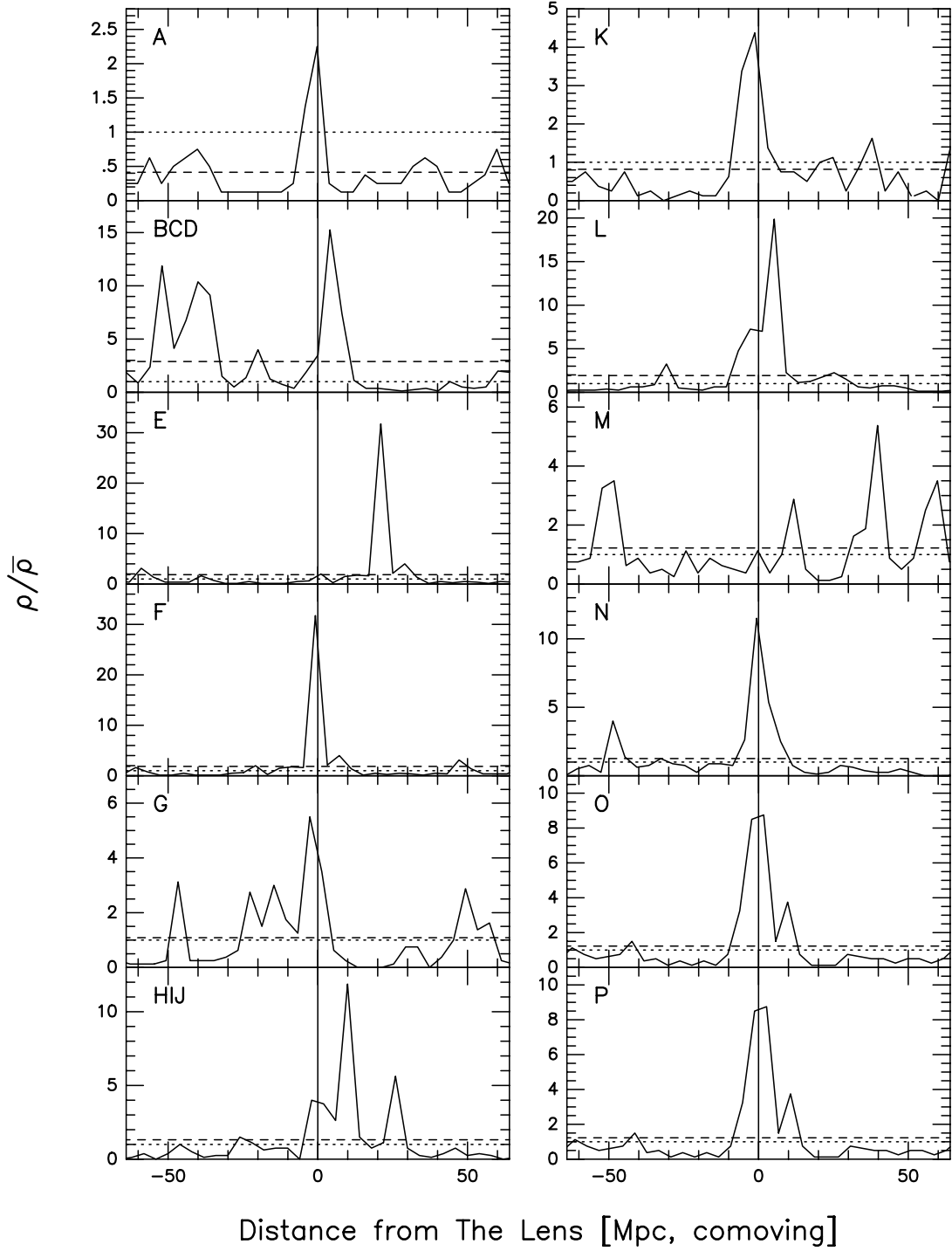


Fig. 6.— Solid curves: density profile  $\rho$  of background matter along line of sight, in units of the universal mean density  $\bar{\rho}$  of the universe, vs. position relative to The Lens. The dotted lines shows the universal mean density. The dashed lines show the mean density along the line of sight. The vertical lines indicate the location of The Lens. All cases are labeled. Notice that for cases B, C, and D, and for cases H, I, and J, The Lens was the same galaxy.

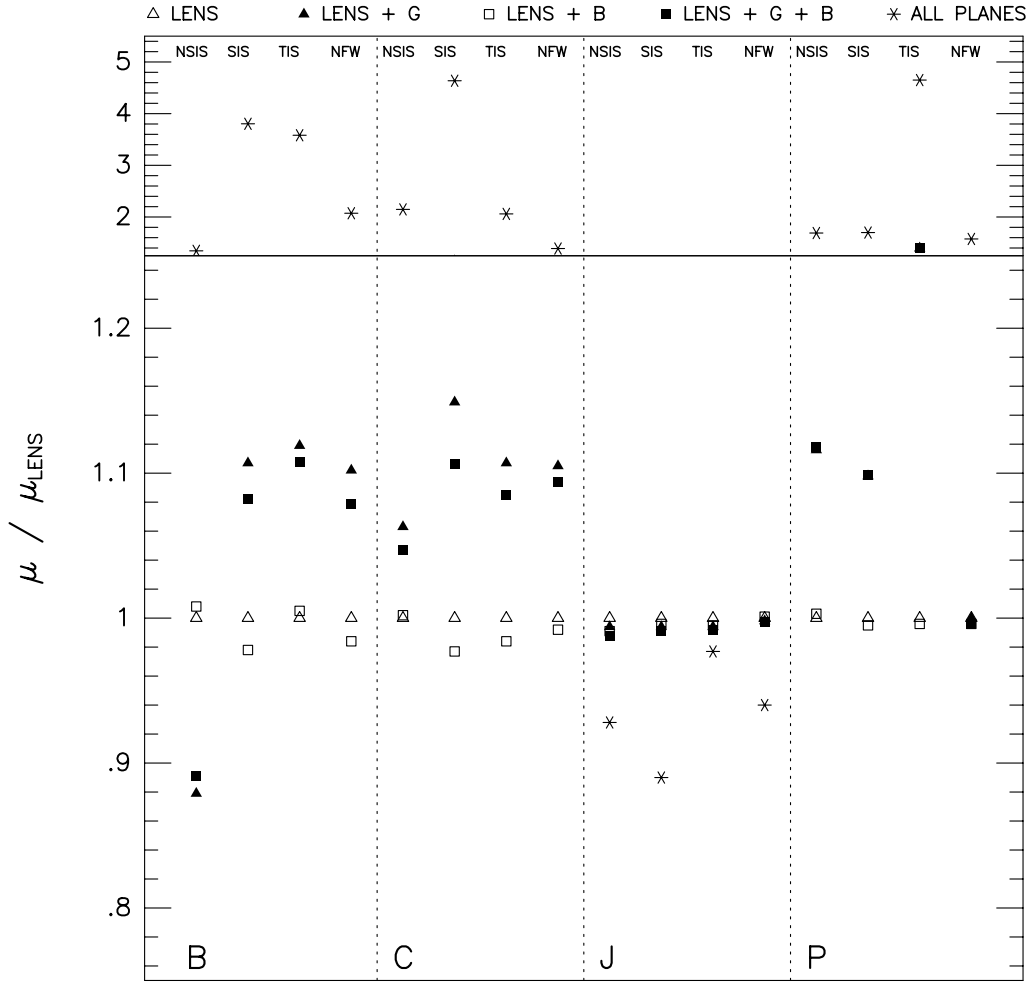


Fig. 7.— Ratio  $\mu/\mu_{\text{Lens}}$ , where  $\mu$  is the magnification and  $\mu_{\text{Lens}}$  is the value of  $\mu$  for the Lens case, for cases B, C, J, and P, with various with various density profiles for galaxies. The various symbols correspond to various types of experiments, as labeled. The various cases are identified by the letters at the bottom of the figure. The density profiles are indicated at the top of the figure.